Phonon thermal conductivity of scandium nitride for thermoelectrics from first-principles calculations and thin-film growth

Sit Kerdsongpanya,[1,*] Olle Hellman,[1,2] Bo Sun,[3] Yee Kan Koh,[3] Jun Lu,[1] Ngo Van Nong,[4] Sergei I. Simak,[1] Björn Alling,[1,5] and Per Eklund[1,†]

[1]*Department of Physics, Chemistry, and Biology (IFM), Linköping University, SE-581 83 Linköping, Sweden*

[2]*Department of Applied Physics and Materials Science, California Institute of Technology, Pasadena, California 91125, USA*

[3]*Department of Mechanical Engineering, National University of Singapore, Block EA, 9 Engineering Drive 1, #07-08, 117576 Singapore*

[4]*Department of Energy Conversion and Storage, Technical University of Denmark, Risø Campus, Frederiksborgvej 399, Building 779, 4000 Roskilde, Denmark*

[5]*Max-Planck-Institut für Eisenforschung GmbH, D-40237 Düsseldorf, Germany*

(Received 2 July 2016; revised manuscript received 6 October 2017; published 9 November 2017)

The knowledge of lattice thermal conductivity of materials under realistic conditions is vitally important since many modern technologies require either high or low thermal conductivity. Here, we propose a theoretical model for determining lattice thermal conductivity, which takes into account the effect of microstructure. It is based on *ab initio* description that includes the temperature dependence of the interatomic force constants and treats anharmonic lattice vibrations. We choose ScN as a model system, comparing the computational predictions to the experimental data by time-domain thermoreflectance. Our experimental results show a trend of reduction in lattice thermal conductivity with decreasing domain size predicted by the theoretical model. These results suggest a possibility to control thermal conductivity by microstructural tailoring and provide a predictive tool for the effect of the microstructure on the lattice thermal conductivity of materials based on *ab initio* calculations.

DOI: 10.1103/PhysRevB.96.195417

Design of modern materials inevitably requires taking the thermal conductivity into account [1]. For thermoelectric materials a low thermal conductivity is crucial to avoid heat transfer across the legs and therefore loss in energy conversion efficiency [2]. In contrast, electronic components require packaging materials with high thermal conductivity to efficiently dissipate the generated heat [3]. Furthermore, the more complex the devices become, the higher is the demand to control the interplay between microstructure and thermal performance [4,5]. For hard protective wear-resistant coatings, in, e.g., cutting or milling applications, thermal properties are often barely considered when optimizing mechanical and tribological properties, despite the fact that the workpiece is typically subject to temperatures locally exceeding 1100 °C in the contact spots [6–8]. The requirements for thermal conductivity are therefore high: the in-plane heat spread within the coating should be as high as possible to ensure uniform heating, while the cross-plane thermal conductivity should be as low as possible to minimize the heat load on the substrate [6–8].These examples underscore how important it is to understand and be able to tailor thermal conductivity in materials in a broad range of applications.

Measurements of thermal conductivity are relatively standard for bulk materials but much more challenging for thin films and nanoscale materials, still being the topic of active method development [9,10]. There is therefore a substantial need to also develop theoretical methods for predicting or simulating the thermal conductivity of real materials. Recent advances in methodology allow us to predict the thermal conductivity from first principles. In the present paper, we combine state-of-the-art computational techniques with characterization and measurements to determine the effect of microstructure on the thermal conductivity of ScN thin films.

When discussing thermal properties from a computational perspective, the lattice dynamical Hamiltonian

$$H = U_0 + \sum_i \frac{p_i^2}{2m_i} + \frac{1}{2!}\sum_{ij\alpha\beta} \Phi_{ij}^{\alpha\beta} u_i^\alpha u_j^\beta + \frac{1}{3!}\sum_{ijk\alpha\beta\gamma} \Phi_{ijk}^{\alpha\beta\gamma} u_i^\alpha u_j^\beta u_k^\gamma + \ldots, \quad (1)$$

is the starting point. It relates the energy of the lattice to displacements (u) of atoms from equilibrium, with a proportionality constant (Φ) for each pair, triplet, quartet, and so on, where ijk are indices of atoms and $\alpha\beta\gamma$ are Cartesian indices. Traditionally, these interatomic force constants Φ are determined by the Taylor expansion of the zero-Kelvin energy around the equilibrium positions, assuming that this expansion is also valid at high temperatures. In this paper, we apply the temperature-dependent effective potential (TDEP) method [11–13], together with *ab initio* molecular dynamics to calculate interatomic force constants Φ. This provides their intrinsic temperature dependence and the ability to model phenomena inaccessible by traditional means [14,15].

To address these general research questions, we choose scandium nitride as a model system. There is an increasing interest in ScN for a wide range of applications [16], such as a dislocation-reducing buffer for group III nitrides [17] or as a potential thermoelectric material because of its relatively large Seebeck coefficient S accompanied by low-resistivity ρ that results in a high thermoelectric power factor (S^2/ρ) of about $2.5-3.3 \times 10^{-3}\,\mathrm{W\,m^{-1}\,K^{-2}}$ [18–21]. ScN can also be made p type by doping on Sc sites [22,23]. The former

*Present address: Department of Materials Science and Engineering, Rensselaer Polytechnic Institute, Troy, New York 12180, USA.

†Corresponding author: per.eklund@liu.se

application requires a high thermal conductivity, while the latter requires it to be low. With an indirect gap of 0.9 eV, the thermal conductivity of ScN will be dominated by the lattice contribution [24–27]. In an ideal harmonic material, nothing prevents phonons from carrying heat. In practice, scattering from impurities or isotopes, grain boundaries, and the intrinsic anharmonicity result in a finite phonon lifetime. Sc is isotopically pure. A large single crystal of pure ScN would leave the intrinsic anharmonicity as the sole scattering mechanism. Any alloying dopant would decrease thermal conductivity more than in a material with natural isotopic defects, as the majority of heat is carried by acoustic phonons, rendering the N isotopic distribution less important. This is therefore an opportunity for tailoring the thermal conductivity, by controlling the microstructure.

The temperature-dependent phonon thermal conductivity of ScN was obtained using TDEP in combination with *ab initio* Born-Oppenheimer molecular dynamics (AIMD). All calculations in this work were carried out using the projector augmented wave method [28] as implemented in the Vienna Ab initio Simulation Package (VASP) [29–32]. The AIMD temperature was set to 400, 800, 1200, and 1600 K and the volumes to 83.74, 88.12, 92.65, 97.34, and 103.82 Å^3 per unit cell for 20 calculations in total, where each calculation was run for 20 000 time steps of 1 fs each with a $5 \times 5 \times 5$ supercell (250 atoms in total). Temperature was controlled with a Nosé-Hoover thermostat [33,34]. The exchange correlation was approximated with the AM05 approximation [35,36] and we used the Γ point for the Brillouin-zone integration along with a plane-wave cutoff of 400 eV. The AIMD data were postprocessed using the TDEP [11–13] and the Gibbs free-energy surface was constructed. From that we extracted volume as a function of temperature, and interpolated the interatomic force constants to the volumes corresponding to zero pressure at the respective temperatures. At these volumes we used the full solution to the linearized phonon Boltzmann equation [37,38] and calculated the lattice contribution to the thermal conductivity on a $31 \times 31 \times 31$ q-point grid.

ScN thin films were grown on one-side-polished sapphire $Al_2O_3(0001)$ (dimensions $10 \times 10 \times 0.5\,\text{mm}^3$) by reactive dc magnetron sputtering in a high-vacuum chamber with a base pressure of 2.7×10^{-5} Pa. The system is described in detail elsewhere [39]. The Sc target was a 7.62-cm-diameter disk shape, with 99.95% purity with fluorine as a common impurity. Prior to deposition, the substrates were degreased in an ultrasonic bath with trichloroethylene, acetone, and isopropanol for 5 min each and subsequently blown dry with N_2. The Sc target was operated in dc mode (power regulated) at a power of 120 W. The substrate was rotated during deposition in order to obtain uniform films. A substrate bias of -30 V bias was applied to the substrate during deposition. The depositions were performed in Ar/N_2 atmosphere at the total gas pressure of 0.67 Pa with 0.27 Pa Ar and 0.4 Pa N_2. Before deposition, the substrates were heated in vacuum to the deposition temperature (for 1 h for temperature stabilization and degassing). The deposition temperatures (T_d) were 400, 500, 600, and 700 °C.

The crystal structure and average characteristic x-ray scattering domain sizes of as-deposited films were determined by x-ray diffraction (XRD) with standard θ-2θ scans using CuKα radiation in a Philips PW 1820 diffractometer. Cross-section transmission electron microscopy (TEM) and plan-view scanning electron microscopy (SEM) were performed on all samples to investigate film microstructure and morphology. For cross-section TEM, the samples were prepared by gluing two pieces of the sample face to face into a Ti grid, then polishing down to 50-μm thickness. Ion milling was performed in a Gatan Precision Ion Polishing System at Ar^+ energy of 5 keV and a gun angle of 5°, with a final polishing step with 2-keV Ar^+ energy and angle of 2°. TEM characterization was performed using a Tecnai G2 TF20UT with a field-emission gun. A ULVAC-RIKO ZEM3 system was used to measure the Seebeck coefficient and electrical resistivity of the films simultaneously in a low-pressure helium atmosphere from room temperature. The error bar of these measurements is within 7%, and the substrate contribution to the Seebeck coefficient and electrical resistivity is negligible.

Thermal conductivities of ScN samples were measured using time-domain thermoreflectance (TDTR). We only briefly describe the measurements here; details of the TDTR setup and implementation can be found in Ref. [40]. Before conducting TDTR measurements, the samples were coated with an ∼80-nm-thick Al as transducer. In TDTR measurements, laser pulses from an ultrafast laser are split into a pump beam and a probe beam. The pump beam is modulated and heats the sample periodically, creating a temperature oscillation in the sample. The probe beam monitors the temperature oscillation at sample surface via thermoreflectance (i.e., change of reflectance with temperature). Since the induced temperature oscillation depends on the thermal properties of the sample, TDTR is an accurate approach to measure the thermal conductance of interface and thermal conductivity of nanostructures [41–43]. In the measurements of ScN samples, we use a $1/e^2$ laser radius of 10 μm, a modulation frequency of 10 MHz, and total laser power of ∼40 mW to limit the steady-state temperature rise to <10 K. The thermal conductivities of ScN and thermal conductance of Al/ScN are then derived by comparing the TDTR measurements to the calculations of the thermal model [44]. In the analysis, the thickness of Al transducer is determined by picosecond acoustics [45] while the heat capacity of ScN is from the literature value of bulk ScN [46]. The measurement uncertainties are estimated to be ∼6% for all measured thermal conductivities.

Figure 1 shows the calculated dynamical structure factor $S(q,E)$ of ScN at room temperature, showing signs of strongly anharmonic behavior. There is a faint satellite peak from the transverse optical (TO) mode around the Γ point, owing to the many available scattering channels between the acoustic and optical branches in this region. This is reminiscent of PbTe and SnTe [15]. While the zone center shows deviations from the assumption that the line shape is Lorentzian (see Supplemental Material [47]), the TO phonons carry little heat and we can therefore assume that the phonon Boltzmann equation is still valid.

At room temperature, using the Boltzmann transport equation for phonons, we predict the lattice contribution to the thermal conductivity to be $20\,\text{Wm}^{-1}\,\text{K}^{-1}$. This is assuming an infinite perfect crystal. This should be compared to previously reported experimental values of $8-12\,\text{Wm}^{-1}\,\text{K}^{-1}$ [19,48]. The reason for these differences is nonideal effects

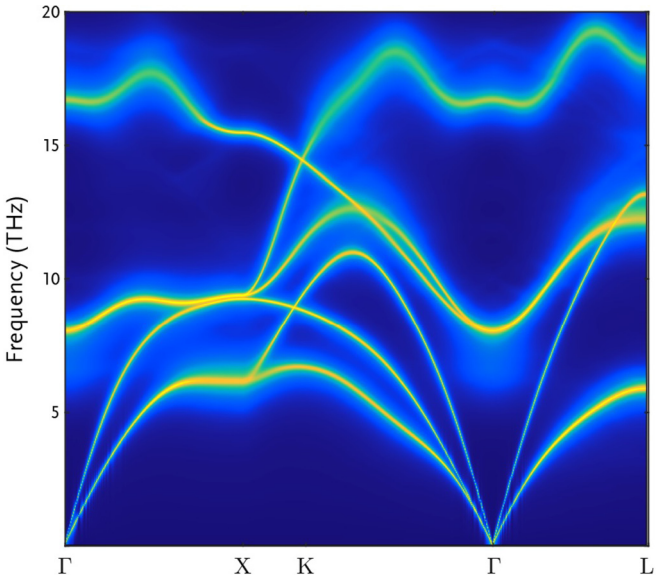

FIG. 1. Dynamical structure factor $S(q,E)$ for ScN at room temperature from first-principles calculations.

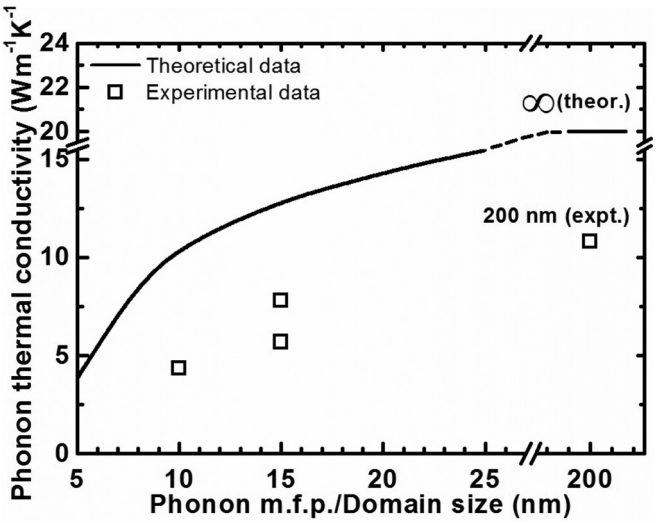

FIG. 2. Theoretical and experimental values of the phonon thermal conductivity of ScN (assuming defect-free crystal) as a function of phonon mean-free path or characteristic x-ray scattering domain size. Error bars for experimental data are stated in the measurement description.

of microstructure (and impurities), i.e., that real ScN is not a perfect crystal. The present synthesis of ScN thin films allows a systematic, and if not quantitative at least semiquantitative, correlation between microstructure and other nonideal effects on thermal conductivity and theoretical calculations of the same effects.

To simulate the microstructural effects, we modify the expression used for the thermal conductivity from

$$\kappa_{\alpha\alpha} = \frac{1}{V}\sum_{\mathbf{q}s} C_{\mathbf{q}s}\upsilon^2_{\alpha\mathbf{q}s}\tau_{\alpha\mathbf{q}s}, \tag{2}$$

where V is the volume, $\upsilon_{\alpha\mathbf{q}s}$ is the mode phonon velocity, $\tau_{\alpha\mathbf{q}s}$ is the lifetime of mode s with wavevector $\boldsymbol{q}$ in Cartesian direction α. κ is determined by an iterative solution to the phonon Boltzmann equation [37,38]. $C_{\mathrm{q}s} = \hbar\omega_{\mathrm{q}s}\partial n^0_{\mathrm{q}s}/\partial T$ is the mode specific heat, where $\hbar$ is the reduced Planck's constant $(h/2\pi)$, $\omega_{\mathbf{q}s}$ is the phonon frequency, and $n^0_{\mathbf{q}s}$ is the Bose-Einstein distribution function. By adding the Heaviside step function $[\Theta(l)]$ as a function of mean scattering domain size l, the thermal conductivity including the domain-size effect is

$$\kappa^{\mathrm{acc}}_{\alpha\alpha}(l) = \frac{1}{V}\sum_{\mathbf{q}s} C_{\mathbf{q}s}\upsilon^2_{\alpha\mathbf{q}s}\tau_{\alpha\mathbf{q}s}\Theta(l - |\upsilon_{\mathbf{q}s}|\tau_{\alpha\mathbf{q}s}). \tag{3}$$

This means that to simulate a certain mean domain size, we only include those phonons whose mean-free path is small enough to fit inside the domain. The results can be seen in Fig. 2, together with the experimental values. The model here differs from other approaches that model interfaces [49–51], phenomenologically compute the phonon lifetime [52], or directly include boundary scattering in the Boltzmann transport equation [53].

XRD results and electron microscopy images of all samples (Figs. 3 and 4) show highly textured polycrystalline ScN films where films were grown in the [111] direction on Al_2O_3 (0001). In addition, the sample grown at deposition temperature (T_d) of 700 °C exhibits epitaxial growth, which can be seen from TEM [Fig. 4(f) and Supplemental Material [47]). Samples grown at $T_d = 400-600$ °C show columnar polycrystalline structure and triangular contrast at the interface between film

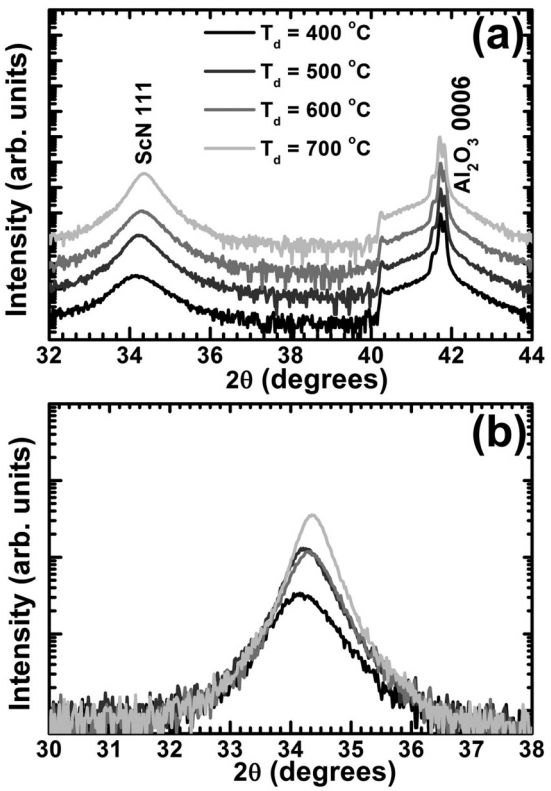

FIG. 3. XRD patterns of ScN films deposited at deposition temperature of $T_d = 400$, 500, 600, and 700 °C on Al_2O_3. (a) Overview and (b) magnified area around the ScN 111 peak.

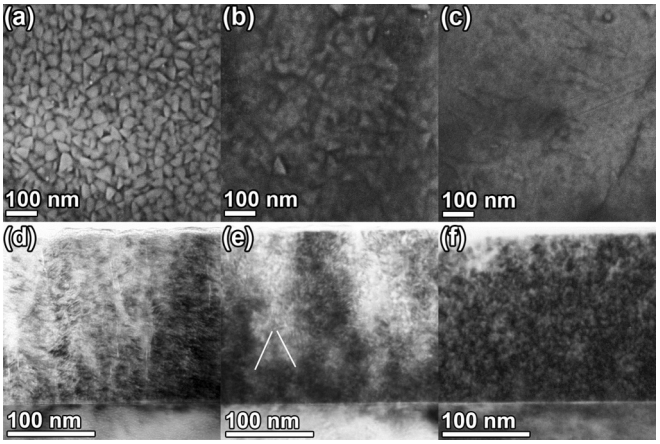

FIG. 4. Electron micrographs of ScN films where (a)–(c) are SEM images and (d)–(f) are cross-section TEM images of the samples that were deposited at deposition temperature, $T_d = 400$, 600, and 700 °C, respectively.

and substrate [Figs. 4(d) and 4(e)]. For more information about samples microstructures see Supplemental Material [47].

From this microstructural information, we see that there are three different types of ScN samples in this study: (1) sample with small domain size, (2) two samples with essentially the same domain size, and (3) epitaxial thin films, where the domain size is the film thickness. For the polycrystalline films, we can use the characteristic x-ray scattering length in θ-2θ geometry (corresponding to the peak broadening) in order to estimate the domain size of the film in the out-of-plane direction. The characteristic x-ray scattering length is defined as the size of the (out-of-plane) coherently diffracting domains. Therefore, we can estimate the average out-of-plane domain size using Scherrer's formula [54]. From the XRD results, the 2θ full width at half maximum of the ScN 111 peaks that are determined by fitting the curve with Lorentz distribution function are 0.80, 0.54, and 0.56° for the polycrystalline films deposited at 400, 500, and 600 °C, respectively. Thus, the estimates of the average out-of-plane domain size of these ScN films are 10, 15, and 15 nm for $T_d = 400$, 500, and 600 °C, respectively. This is consistent with transmission electron microscopy (see Fig. S4 in Supplemental Material [47]).

All ScN films were grown to the same thickness of about 200 nm (see Fig. S2 in Supplemental Material [47]). The phonon thermal conductivity of all the samples was determined from $\kappa_{ph} = \kappa_{tot} - \kappa_e$, where κ_{tot} is the total thermal conductivity and κ_e is the electronic thermal conductivity, which is described as $\kappa_e = LT/\rho$ where L is the Lorenz number ($2.44 \times 10^{-8}\,\mathrm{W\,\Omega\,K^{-2}}$), ρ is the electrical resistivity, and T is the absolute temperature. The electrical resistivity of the polycrystalline ScN films at room temperature is 61.0, 11.0, and 9.8 $\mu\Omega$m for the films deposited at 400, 500, and 600 °C, respectively. For the epitaxial film, the electrical resistivity is 4.0 $\mu\Omega$m. From the $\kappa_{ph} = \kappa_{tot} - \kappa_e$ equation, we can calculate the phonon thermal conductivity from the measured total thermal conductivity at room temperature for all ScN films. The results are shown in Fig. 2. For polycrystalline films, the phonon thermal conductivity of the samples with domain sizes of 10 and 15 nm (two samples) are 5.4, 9.7, and 7.1 $\mathrm{W\,m^{-1}\,K^{-1}}$, respectively. The origin of the slight difference in phonon thermal conductivity between the two 15-nm-domain-size samples is likely correlated with the fact that the thermal conductance of the Al/ScN interface of the 600 °C sample is also particularly low (see Fig. S3 in Supplemental Material [47]). This indicates that the quality of the sample (in terms of surface oxidation and/or impurity content) is not as good compared to other samples. On the other hand, the epitaxial film exhibits a phonon thermal conductivity of 10.5 $\mathrm{Wm^{-1}\,K^{-1}}$ which is similar to previous values reported for epitaxial ScN films [19,55].

Overall, the results show an increase of phonon thermal conductivity with increasing domain size. These results agree well with our calculated phonon thermal conductivity, but with a systematic difference of a factor of ~2. For example, the predicted phonon thermal conductivity of a polycrystalline film with 10-nm domain size is ~10.3 $\mathrm{Wm^{-1}\,K^{-1}}$, while the experimental value is ~5.4 $\mathrm{Wm^{-1}\,K^{-1}}$. The reason for this systematic shift is additional effects, other than domain-size effect, that are not accounted for in the model. Including film thickness and impurity scattering reduces the calculated values close to the experimental ones. Oxygen impurities on N sites (known in ScN films) require high concentrations to affect the thermal conductivity. A concentration of 5 at. % oxygen only reduces thermal conductivity by at most 1% at 300 K. However, since Sc is isotopically pure, any impurities on Sc sites will have a substantial effect on thermal conductivity. Introduction of a fraction of a percent of vacancies, antisite, or substitutional defects (data not shown, as we do not have experimental information on the concentration of Sc-site defects) decreases the phonon lifetimes for the Sc-dominated acoustic branches substantially, lowering the lattice thermal conductivity by as much as 50%. These results and observations validate the model for calculating effects of microstructure on thermal conductivity and enable comparisons of measurements of thermal conductivity of real materials with calculations separating different effects.

In conclusion, we have theoretically and experimentally investigated phonon thermal conductivity in ScN thin films. Using a theoretical model accounting for microstructural effects on the thermal conductivity, we can semiquantitatively predict the thermal conductivity of ScN. The predictions systematically overestimate the thermal conductivity by a factor of ~2, which is due to additional effects, including impurity scattering, which can in principle also be incorporated into the model to improve the quantitative agreement. The dominant effect is domain-size reduction of the thermal conductivity as evidenced by the calculated values of 20 $\mathrm{Wm^{-1}\,K^{-1}}$ for an ideal single crystal and 4−13 $\mathrm{Wm^{-1}\,K^{-1}}$ for domain sizes of 5–20 nm. This large reduction in thermal conductivity with grain size agrees well with our experiments on ScN, and more generally offers an approach for integrated theoretical-experimental design of the thermal conductivity of real materials.

The research leading to these results has received funding from the European Research Council under the European Community's Seventh Framework Programme (Grant No. FP/2007-2013)/ERC Grant Agreement No. 335383, the

Swedish Government Strategic Research Area in Materials Science on Functional Materials at Linköping University (Faculty Grant SFO-Mat-LiU No. 2009 00971), the Swedish Research Council (VR) under Projects No. 2012–4430 and No. 2016–03365 (S.K. and P.E.), No. 330-2014-6336 (B.A.), No. 2014–4750 (S.I.S.), No. 637-2013-7296 (O.H.), the Linnaeus Environment LiLi-NFM, and the Swedish Foundation for Strategic Research (SSF) through the Future Research Leaders 5 Program. The calculations were performed using computer resources provided by the Swedish National Infrastructure for Computing (SNIC) at the National Supercomputer Centre (NSC). N.V.N. would like to acknowledge the financial support by the NanoCaTe project (FP7-NMP No. 604647). B.S. and Y.K.K. acknowledge the National University of Singapore Startup Grant.

S.K. and O.H. contributed equally to this work.

[1] E. S. Toberer, L. L. Baranowski, and C. Dames, Advances in thermal conductivity, Annu. Rev. Mater. Res. **42**, 179 (2012).

[2] G. J. Snyder and E. S. Toberer, Complex thermoelectric materials, Nat. Mater. **7**, 105 (2008).

[3] X. S. Liu, M. H. Hu, C. G. Caneau, R. Bhat, and C.-E. Zah, Thermal management strategies for high power semiconductor pump lasers, IEEE Trans. Compon. Packag. Technol. **29**, 268 (2006).

[4] R. Cheaito, J. C. Duda, T. E. Beechem, K. Hattar, J. F. Ihlefeld, D. L. Medlin, M. A. Rodriguez, M. J. Campion, E. S. Piekos, and P. E. Hopkins, Experimental Investigation of Size Effects on the Thermal Conductivity of Silicon-Germanium Alloy Thin Films, Phys. Rev. Lett. **109**, 195901 (2012).

[5] C. J. Vineis, A. Shakouri, A. Majumdar, and M. G. Kanatzidis, Nanostructured thermoelectrics: Big efficiency gains from small features, Adv. Mater. **22**, 3970 (2010).

[6] P. H. M. Böttger, E. Lewin, J. Patscheider, V. Shklover, D. G. Cahill, R. Ghisleni, and M. Sobiech, Thermal conductivity of hard oxynitride coatings, Thin Solid Films **549**, 232 (2013).

[7] P. H. M. Böttger, A. V. Gusarov, V. Shklover, J. Patscheider, and M. Sobiech, Anisotropic layered media with microinclusions: Thermal properties of arc-evaporation multilayer metal nitrides, Int. J. Therm. Sci. **77**, 75 (2014).

[8] P. H. M. Böttger, L. Braginsky, V. Shklover, E. Lewin, J. Patscheider, D. G. Cahill, and M. Sobiech, Hard wear-resistant coatings with anisotropic thermal conductivity for high thermal load applications, J. Appl. Phys. **116**, 013507 (2014).

[9] D. G. Cahill, W. K. Ford, K. E. Goodson, G. D. Mahan, A. Majumdar, H. J. Maris, R. Merlin, and S. R. Phillpot, Nanoscale thermal transport, J. Appl. Phys. **93**, 793 (2003).

[10] D. G. Cahill, P. V. Braun, G. Chen, D. R. Clarke, S. Fan, K. E. Goodson, P. Keblinski, W. P. King, G. D. Mahan, A. Majumdar, H. J. Maris, S. R. Phillpot, E. Pop, and L. Shi, Nanoscale thermal transport. II. 2003–2012, Appl. Phys. Rev. **1**, 011305 (2014).

[11] O. Hellman, I. A. Abrikosov, and S. I. Simak, Lattice dynamics of anharmonic solids from first principles, Phys. Rev. B **84**, 180301 (2011).

[12] O. Hellman and I. A. Abrikosov, Temperature-dependent effective third-order interatomic force constants from first principles, Phys. Rev. B **88**, 144301 (2013).

[13] O. Hellman, P. Steneteg, I. A. Abrikosov, and S. I. Simak, Temperature dependent effective potential method for accurate free energy calculations of solids, Phys. Rev. B **87**, 104111 (2013).

[14] J. D. Budai, J. Hong, M. E. Manley, E. D. Specht, C. W. Li, J. Z. Tischler, D. L. Abernathy, A. H. Said, B. M. Leu, L. A. Boatner, R. J. McQueeney, and O. Delaire, Metallization of vanadium dioxide driven by large phonon entropy, Nature (London) **515**, 535 (2014).

[15] C. W. Li, O. Hellman, J. Ma, A. F. May, H. B. Cao, X. Chen, A. D. Christianson, G. Ehlers, D. J. Singh, B. C. Sales, and O. Delaire, Phonon Self-Energy and Origin of Anomalous Neutron Scattering Spectra in SnTe and PbTe Thermoelectrics, Phys. Rev. Lett. **112**, 175501 (2014).

[16] S. W. King, R. F. Davis, and R. J. Nemanich, Gas source molecular beam epitaxy of scandium nitride on silicon carbide and gallium nitride surfaces, J. Vac. Sci. Technol. A **32**, 061504 (2014).

[17] M. J. Kappers, M. A. Moram, Y. Zhang, M. E. Vickers, Z. H. Barber, and C. J. Humphreys, Interlayer methods for reducing the dislocation density in gallium nitride, Physica B **401–402**, 296 (2007).

[18] S. Kerdsongpanya, N. Van Nong, N. Pryds, A. Žukauskaitė, J. Jensen, J. Birch, J. Lu, L. Hultman, G. Wingqvist, and P. Eklund, Anomalously high thermoelectric power factor in epitaxial ScN thin films, Appl. Phys. Lett. **99**, 232113 (2011).

[19] P. V. Burmistrova, J. Maassen, T. Favaloro, B. Saha, S. Salamat, Y. Rui Koh, M. S. Lundstrom, A. Shakouri, and T. D. Sands, Thermoelectric properties of epitaxial ScN films deposited by reactive magnetron sputtering onto MgO(001) substrates, J. Appl. Phys. **113**, 153704 (2013).

[20] P. Eklund, S. Kerdsongpanya, and B. Alling, Transition-metal-nitride-based thin films as novel energy harvesting materials, J. Mater. Chem. C **4**, 3905 (2016).

[21] P. V. Burmistrova, D. N. Zakharov, T. Favaloro, A. Mohammed, E. A. Stach, A. Shakouri, and T. D. Sands, Effect of deposition pressure on the microstructure and thermoelectric properties of epitaxial ScN(001) thin films sputtered onto MgO(001) substrates, J. Mater. Res. **30**, 626 (2015).

[22] B. Saha, M. Garbrecht, J. A. Perez-Taborda, M. H. Fawey, Y. R. Koh, A. Shakouri, M. Martin-Gonzalez, L. Hultman, and T. D. Sands, Compensation of native donor doping in ScN: Carrier concentration control and *p*-type ScN, Appl. Phys. Lett. **110**, 252104 (2017).

[23] B. Saha, G. Naik, V. Drachev, A. Boltasseva, E. E. Marinero, and T. D. Sands, Electronic and optical properties of ScN and (Sc,Mn)N thin films deposited by reactive DC-magnetron sputtering, J. Appl. Phys. **114**, 063519 (2013).

[24] H. A. H. Al-Brithen, A. R. Smith, and D. Gall, Surface and bulk electronic structure of ScN(001) investigated by scanning tunneling microscopy/spectroscopy and optical absorption spectroscopy, Phys. Rev. B **70**, 045303 (2004).

[25] S. Kerdsongpanya, B. Alling, and P. Eklund, Effect of point defects on the electronic density of states of ScN studied by first-principles calculations and implications for thermoelectric properties, Phys. Rev. B **86**, 195140 (2012).

[26] S. Kerdsongpanya, B. Alling, and P. Eklund, Phase stability of ScN-based solid solutions for thermoelectric applications from first-principles calculations, J. Appl. Phys. **114**, 073512 (2013).
[27] C. Li and D. Broido, Phonon thermal transport in transition-metal and rare-earth nitride semiconductors from first principles, Phys. Rev. B **95**, 205203 (2017).
[28] P. E. Blöchl, Projector augmented-wave method, Phys. Rev. B **50**, 17953 (1994).
[29] G. Kresse and J. Hafner, Ab initio molecular dynamics for open-shell transition metals, Phys. Rev. B **48**, 13115 (1993).
[30] G. Kresse and D. Joubert, From ultrasoft pseudopotentials to the projector augmented-wave method, Phys. Rev. B **59**, 1758 (1999).
[31] G. Kresse and J. Furthmüller, Efficient iterative schemes for ab initio total-energy calculations using a plane-wave basis set, Phys. Rev. B **54**, 11169 (1996).
[32] G. Kresse and J. Furthmüller, Efficiency of ab-initio total energy calculations for metals and semiconductors using a plane-wave basis set, Comput. Mater. Sci. **6**, 15 (1996).
[33] S. Nosé, A molecular dynamics method for simulations in the canonical ensemble, Mol. Phys. **52**, 255 (1984).
[34] W. G. Hoover, Canonical dynamics: Equilibrium phase-space distributions, Phys. Rev. A **31**, 1695 (1985).
[35] R. Armiento and A. E. Mattsson, Functional designed to include surface effects in self-consistent density functional theory, Phys. Rev. B **72**, 085108 (2005).
[36] A. E. Mattsson and R. Armiento, Implementing and testing the AM05 spin density functional, Phys. Rev. B **79**, 155101 (2009).
[37] A. Ward, D. A. Broido, D. A. Stewart, and G. Deinzer, Ab initio theory of the lattice thermal conductivity in diamond, Phys. Rev. B **80**, 125203 (2009).
[38] M. Omini and A. Sparavigna, An iterative approach to the phonon Boltzmann equation in the theory of thermal conductivity, Physica B **212**, 101 (1995).
[39] F. Eriksson, G. A. Johansson, H. M. Hertz, and J. Birch, Enhanced soft x-ray reflectivity of Cr/Sc multilayers by ion-assisted sputter deposition, Opt. Eng. **41**, 2903 (2002).
[40] B. Sun and Y. K. Koh, Understanding and eliminating artifact signals from diffusely scattered pump beam in measurements of rough samples by time-domain thermoreflectance (TDTR), Rev. Sci. Instrum. **87**, 064901 (2016).
[41] O. Cometto, B. Sun, S. H. Tsang, X. Huang, Y. K. Koh, and E. H. T. Teo, Vertically self-ordered orientation of nanocrystalline hexagonal boron nitride thin films for enhanced thermal characteristics, Nanoscale **7**, 18984 (2015).
[42] J. Ju, B. Sun, G. Haunschild, B. Loitsch, B. Stoib, M. S. Brandt, M. Stutzmann, Y. K. Koh, and G. Koblmüller, Thermoelectric properties of In-rich InGaN and InN/InGaN superlattices, AIP Adv. **6**, 045216 (2016).
[43] B. Huang and Y. K. Koh, Improved topological conformity enhances heat conduction across metal contacts on transferred graphene, Carbon **105**, 268 (2016).
[44] D. G. Cahill, Analysis of heat flow in layered structures for time-domain thermoreflectance, Rev. Sci. Instrum. **75**, 5119 (2004).
[45] C. Thomsen, H. T. Grahn, H. J. Maris, and J. Tauc, Surface generation and detection of phonons by picosecond light pulses, Phys. Rev. B **34**, 4129 (1986).
[46] B. Saha, J. Acharya, T. D. Sands, and U. V. Waghmare, Electronic structure, phonons, and thermal properties of ScN, ZrN, and HfN: A first-principles study, J. Appl. Phys. **107**, 033715 (2010).
[47] See Supplemental Material at http://link.aps.org/supplemental/10.1103/PhysRevB.96.195417 for additional microstructural and electrical/thermal characterization, and information about phonon self-energy calculations.
[48] V. Rawat, D. N. Zakharov, E. A. Stach, and T. D. Sands, Pseudomorphic stabilization of rocksalt GaN in TiN/GaN multilayers and superlattices, Phys. Rev. B **80**, 024114 (2009).
[49] H.-S. Kim, S. D. Kang, Y. Tang, R. Hanus, and G. J. Snyder, Dislocation strain as the mechanism of phonon scattering at grain boundaries, Mater. Horiz. **3**, 234 (2016).
[50] P. Hołuj, C. Euler, B. Balke, U. Kolb, G. Fiedler, M. M. Müller, T. Jaeger, E. Chávez Angel, P. Kratzer, and G. Jakob, Reduced thermal conductivity of TiNiSn/HfNiSn superlattices, Phys. Rev. B **92**, 125436 (2015).
[51] P. Chen, N. A. Katcho, J. P. Feser, W. Li, M. Glaser, O. G. Schmidt, D. G. Cahill, N. Mingo, and A. Rastelli, Role of Surface-Segregation-Driven Intermixing on the Thermal Transport through Planar Si/Ge Superlattices, Phys. Rev. Lett. **111**, 115901 (2013).
[52] N. Mingo and D. A. Broido, Length dependence of carbon nanotube thermal conductivity and the problem of long waves, Nano Lett. **5**, 1221 (2005).
[53] G. Fugallo, M. Lazzeri, L. Paulatto, and F. Mauri, Ab initio variational approach for evaluating lattice thermal conductivity, Phys. Rev. B **88**, 045430 (2013).
[54] M. Birkholz, *Thin Film Analysis by X-Ray Scattering* (Wiley-VCH, Weinheim, 2006).
[55] V. Rawat, Y. K. Koh, D. G. Cahill, and T. D. Sands, Thermal conductivity of (Zr,W)N/ScN, J. Appl. Phys. **105**, 024909 (2009).